Atmospheric Environment 187 (2018) 381–389

Contents lists available at ScienceDirect

Atmospheric Environment

journal homepage: www.elsevier.com/locate/atmosenv

Large-eddy simulation of reactive pollutant exchange at the top of a street canyon

Beom-Soon Han[a], Jong-Jin Baik[a,*], Kyung-Hwan Kwak[b], Seung-Bu Park[c]

[a] School of Earth and Environmental Sciences, Seoul National University, Seoul, South Korea
[b] School of Natural Resources and Environmental Science, Kangwon National University, Chuncheon, South Korea
[c] Center for Climate Physics, Institute for Basic Science, Busan, South Korea

ARTICLE INFO

Keywords:
Reactive pollutant exchange
Chemical reaction
Street canyon
Large-eddy simulation

ABSTRACT

The exchange of reactive pollutants (NO, NO_2, and O_3) at the top (roof level) of a street canyon are investigated using the parallelized large-eddy simulation model (PALM). The transport equations of NO, NO_2, and O_3 with simple photochemical reactions are combined within the LES model for this study. NO and NO_2 are emitted from an area source located near the canyon floor, and O_3 is included within the ambient air and inflow. A clockwise-rotating vortex appears in the street canyon and transports NO, NO_2, and O_3. NO and NO_2 are transported along the ground and leeward wall and escape from the canyon at the roof level. O_3 enters the canyon at the roof level and is transported along the windward wall. The mean O_3 production rate is generally negative with large magnitudes at and near the roof level and near the windward wall. The chemical reactions reduce the mean NO and O_3 concentrations in the canyon by 31% and 84%, respectively, and increase the mean NO_2 concentration in the canyon by 318%. The exchange of reactive pollutants at the roof level is significantly affected by small-scale eddies at the roof level and low- or high-speed streaks above the canyon. Air in the canyon with high NO and NO_2 concentrations escapes from the canyon when low-speed air parcel appears due to small-scale eddies at the roof level or low-speed streak above the canyon. In contrast, air outside the canyon with a high O_3 concentration enters the canyon when high-speed air parcel appears because of small-scale eddies at the roof level or high-speed streak above the canyon. The time-lagged correlation analysis reveals that NO, NO_2, and O_3 concentrations near the ground are affected by low- or high-speed streaks above the canyon but not significantly affected by small-scale eddies at the roof level.

1. Introduction

With the increasing awareness of urban air pollution and its impacts on health, flow and pollutant dispersion in urban street canyons have been widely investigated in recent decades. Field observations (Rotach, 1995; Allwine et al., 2002; Nelson et al., 2011), wind tunnel experiments (Pavageau and Schatzmann, 1999; Kastner-Klein et al., 2001; Allegrini et al., 2013), and numerical model simulations (Baik and Kim, 2002; Kwak and Baik, 2012, 2014; Kim et al., 2012; Park et al., 2015; Sanchez et al., 2016; Moradpour et al., 2018) have been performed to better understand flow and pollutant dispersion in street canyons. In particular, numerical modeling is a very useful tool for such investigations, because numerical models can provide data with high spatial and temporal resolutions. Comprehensive reviews of numerical modeling of flow and pollutant dispersion in street canyons are given in Li et al. (2006) and Zhong et al. (2016).

Large-eddy simulation (LES) models have been used to study turbulent flow in urban street canyons. Cui et al. (2004) examined turbulent flow in a street canyon using an LES model and found that a large clockwise-rotating vortex appears in a street canyon and flow is more turbulent near the windward wall than near the leeward wall. They also found that flow at the roof level is intermittent and multi-scale turbulent events affect flow at the roof level. Letzel et al. (2008) showed that turbulence generated by wind shear dominates at the roof level and makes the circulation in a street canyon intermittent and unstable. Park et al. (2012) examined turbulent flow in a street canyon with heating of the windward wall, canyon floor or leeward wall. Heating of the canyon floor or leeward wall strengthens a large clockwise-rotating vortex in the canyon. In contrast, heating of the windward wall makes the clockwise-rotating vortex small and induces updrafts near the windward wall. Heating of the windward wall, canyon floor or leeward wall increases both turbulent kinetic energy and magnitude of vertical turbulent momentum flux at the roof level.

In addition to turbulent flow, passive pollutant dispersion in urban

* Corresponding author. School of Earth and Environmental Sciences, Seoul National University, Seoul 08826, South Korea.
E-mail address: jjbaik@snu.ac.kr (J.-J. Baik).

https://doi.org/10.1016/j.atmosenv.2018.06.012
Received 19 February 2018; Received in revised form 18 May 2018; Accepted 10 June 2018
Available online 14 June 2018
1352-2310/

street canyons has been widely studied using LES models. Michioka et al. (2011) examined the process of pollutant removal from a street canyon using an LES model. They found that small vortices at the roof level and low-momentum fluid above the canyon dominate the process of pollutant removal from the street canyon. Chung and Liu (2013) examined the effects of aspect ratio (i.e., the ratio of building height to canyon width) on pollutant removal from street canyons. They found that when the aspect ratio is larger than 0.5, the amount of pollutant escaped from the canyon decreases as the aspect ratio increases. When the aspect ratio is less than 0.5, pollutant escaped from the canyon re-enters the canyon and a change in aspect ratio does not affect the amount of escaped pollutant significantly. Liu and Wong (2014) noted that vertical turbulent pollutant flux is larger than vertical mean pollutant flux at the roof level, except near the windward wall. This means that pollutant emitted near the ground is escaped at the roof level by turbulent eddies rather than by mean flow.

The aforementioned LES studies investigated dispersion of passive pollutant. Pollutants emitted in real urban areas are, however, chemically reactive. Considering this point, LES studies of air pollution in street canyons which couple dynamics and chemistry have been performed (Grawe et al., 2007; Zhong et al., 2015). Baker et al. (2004) combined simple photochemical reactions of nitric oxide (NO), nitrogen dioxide (NO_2), and ozone (O_3) within an LES model to examine dispersion of reactive pollutants in a street canyon. They found that NO and NO_2 concentrations are high near the ground and leeward wall and O_3 is entrained into the canyon near the windward wall, resulting in high O_3 concentration near the windward wall. They also found that vigorous O_3 decomposition occurs near the ground and windward wall, while the center of the canyon reaches a chemical equilibrium. Zhong et al. (2017) investigated reactive pollutant dispersion in a deep street canyon using an LES model coupled with complex chemistry of O_3, NO_x (= NO + NO_2), and volatile organic compounds (VOCs). They found that NO_2 and O_3 concentrations in the street canyon in the simulation with the complex chemical reactions are increased by approximately 30–40% compared to those in the simulation with simple chemistry of NO, NO_2, and O_3. They also found that mixing of chemical species is incomplete in the street canyon, i.e., chemical species are segregated from each other. This segregation of chemical species interrupts conversion of NO to NO_2. Kikumoto and Ooka (2012) examined dispersion of reactive pollutants at the roof level using an LES model and found that reactive pollutants escape from the canyon when flow speed becomes slow at the roof level. In contrast, entrance of reactive pollutants from outside the canyon occurs when flow speed becomes fast at the roof level. However, they did not investigate the effects of turbulent structures (e.g., small vortices and low- or high-speed streaks) on reactive pollutant dispersion. Turbulent structures can significantly affect flow speed at the roof level and hence reactive pollutant dispersion. Along with the line of these previous LES studies and as an extension of those studies, it would be interesting to further investigate the relationship between turbulent structures and reactive pollutant exchange at the roof level. This motivates the present study.

In this study, the effects of turbulence on reactive pollutant exchange at the roof level are investigated. Descriptions of an LES model and simulation design are presented in section 2. In section 3, the LES model is validated and simulation results are presented and discussed. In section 4, a summary and conclusions are given.

2. LES model and simulation design

The parallelized LES model (PALM, Maronga et al., 2015) version 4.0 is used in this study. In PALM, the filtered Navier-Stokes equations under the Boussinesq approximation are used. The momentum equation, mass continuity equation, thermodynamic energy equation, and subgrid-scale (SGS) turbulent kinetic energy equation are solved. For the parameterization of SGS turbulent fluxes, the 1.5-order Deardorff (1980) scheme is used. The third-order Runge-Kutta scheme and the fifth-order upwind scheme (Wicker and Skamarock, 2002) are used for time integration and advection terms, respectively.

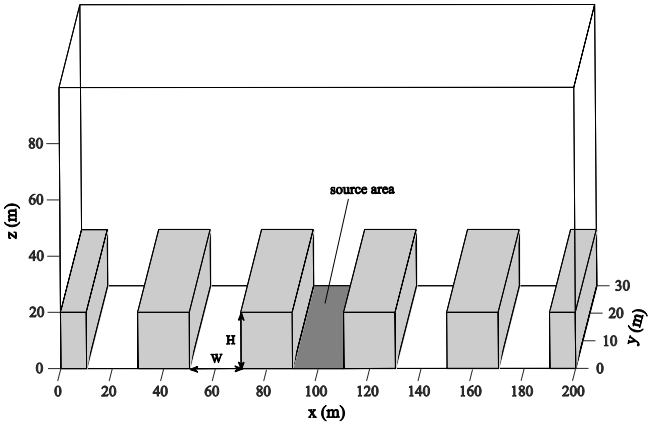

Fig. 1. An illustration of the computational domain. H and W represent the building height and the width of the street canyon, respectively. NO and NO_2 are emitted in the source area located at the center of the computational domain.

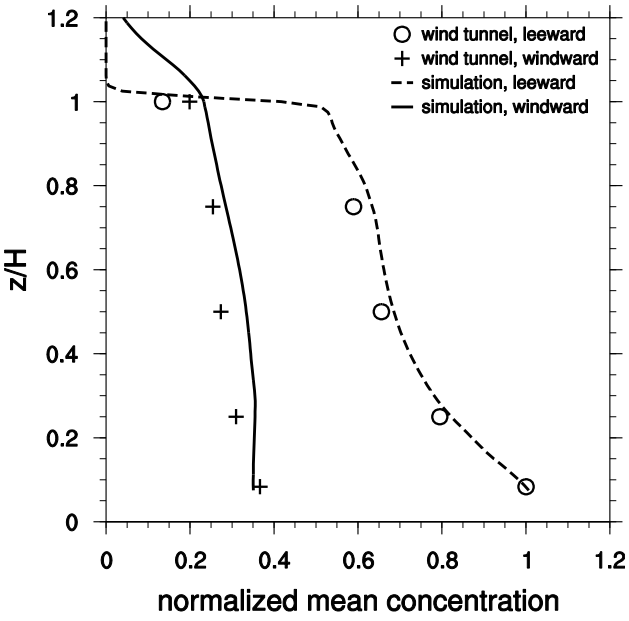

Fig. 2. Vertical profiles of sum of time-averaged NO and NO_2 concentrations (the present simulation result) and passive scalar (the wind tunnel experiment result of Pavageau and Schatzmann (1999)) near the windward and leeward walls (0.03H from each wall). The results of the simulation and wind tunnel experiment are normalized by the concentration near the leeward wall at z = 0.08H (Kikumoto and Ooka, 2012). Solid and dashed lines represent the simulation result near the windward and leeward walls, respectively. Cross and open circle represent the wind tunnel experiment result near the windward and leeward walls, respectively.

For this study, the transport equations of NO, NO_2, and O_3 are implemented into PALM. The simple photochemical reactions for NO, NO_2, and O_3 are as follows (Seinfeld and Pandis, 2006):

$$NO_2 + h\nu \rightarrow NO + O, \quad (1)$$

$$O + O_2 + M \rightarrow O_3 + M, \quad (2)$$

$$O_3 + NO \rightarrow NO_2 + O_2. \quad (3)$$

In Eq. (2), M denotes a molecule that absorbs energy and stabilizes O_3, and $h\nu$ denotes a photon of sunlight of frequency ν.

The filtered transport equations of NO, NO_2, and O_3 are expressed

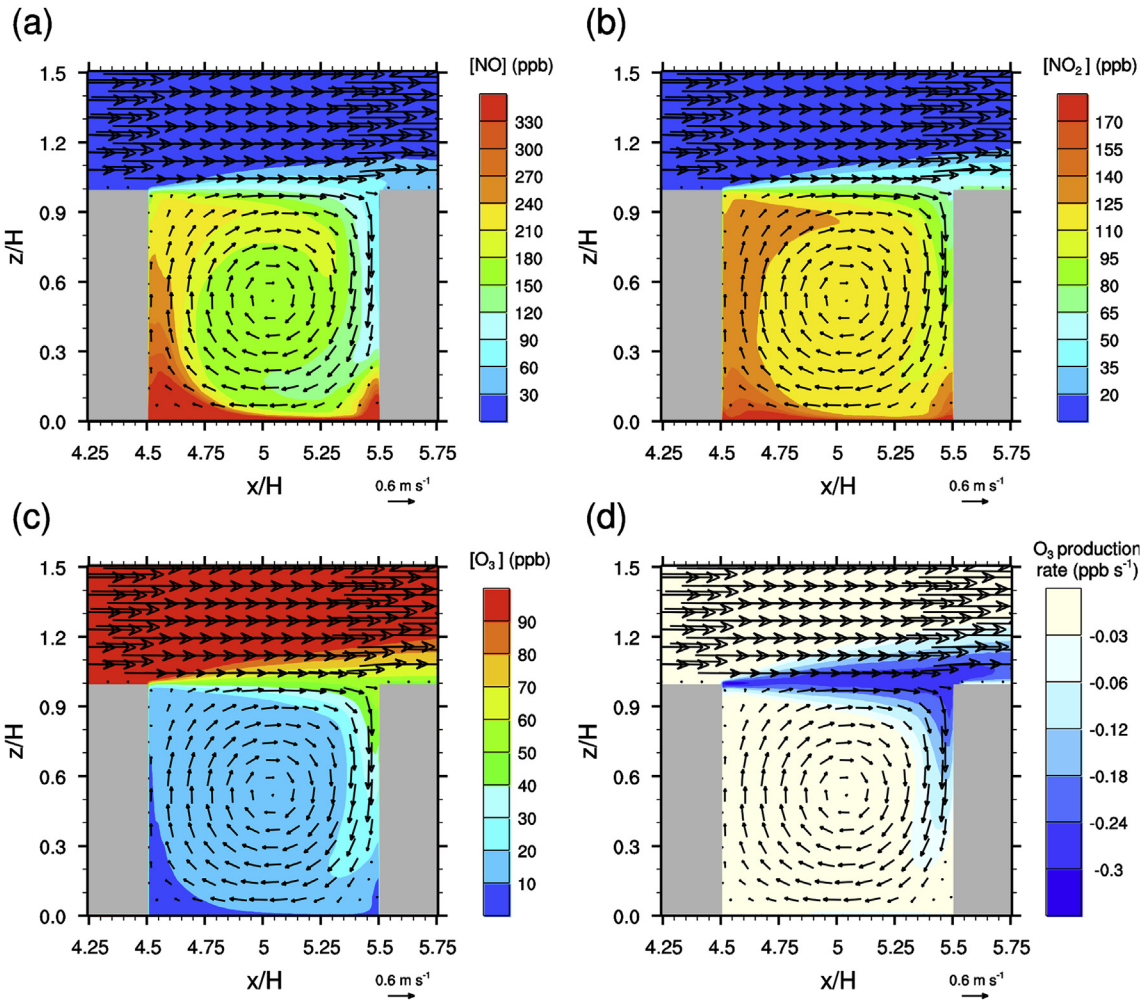

Fig. 3. Fields of mean velocity vector, (a) NO, (b) NO_2, and (c) O_3 concentrations, and (d) the O_3 production rate on the x–z plane at y = 15 m.

as:

$$\frac{\partial \overline{[NO]}}{\partial t} + \frac{\partial}{\partial x_j}(\overline{u_j}\,\overline{[NO]}) = -\frac{\partial}{\partial x_j}(\overline{u''_j [NO]'}) + J_{NO_2}\overline{[NO_2]} - k_1\overline{[O_3]}\,\overline{[NO]} + +S_{NO}, \quad (4)$$

$$\frac{\partial \overline{[NO_2]}}{\partial t} + \frac{\partial}{\partial x_j}(\overline{u_j}\,\overline{[NO_2]}) = -\frac{\partial}{\partial x_j}(\overline{u''_j [NO_2]'}) - J_{NO_2}\overline{[NO_2]} + k_1\overline{[O_3]}\,\overline{[NO]} + S_{NO_2}, \quad (5)$$

$$\frac{\partial \overline{[O_3]}}{\partial t} + \frac{\partial}{\partial x_j}(\overline{u_j}\,\overline{[O_3]}) = -\frac{\partial}{\partial x_j}(\overline{u''_j [O_3]'}) + k_2\overline{[O]}\,\overline{[O_2]}\,\overline{[M]} - k_1\overline{[O_3]}\,\overline{[NO]}, \quad (6)$$

where overbar and u_j (j = 1, 2, 3) represent the filtered variable and the velocities in the j-directions, respectively. Double prime denotes the SGS variable. J_{NO_2}, k_1, and k_2 are the photolysis rate of NO_2 in Eq. (1), the rate constant in Eq. (3), and the rate constant in Eq. (2), respectively. S_{NO} and S_{NO_2} denote the source terms of NO and NO_2, respectively. Square bracket represents the pollutant concentration in ppb. The formation rate of O by Eq. (1) is approximately the depletion rate of O by Eq. (2) due to the high reactivity of O (pseudo-steady-state approximation) (Seinfeld and Pandis, 2006). Therefore,

$$J_{NO_2}\overline{[NO_2]} = k_2\overline{[O]}\,\overline{[O_2]}\,\overline{[M]}. \quad (7)$$

By substituting Eq. (7) into Eq. (6), the following equation is obtained:

$$\frac{\partial \overline{[O_3]}}{\partial t} + \frac{\partial}{\partial x_j}\left(\overline{u_j}\,\overline{[O_3]}\right) = -\frac{\partial}{\partial x_j}(\overline{u''_j [O_3]''}) + J_{NO_2}\overline{[NO_2]} - k_1\overline{[O_3]}\,\overline{[NO]}. \quad (8)$$

The photolysis rate J_{NO_2} and the rate constant k_1 are calculated following previous studies (Shetter et al., 1988; Baker et al., 2004; Baik et al., 2007). J_{NO_2} and k_1 are specified as 0.00816 s^{-1} and 0.000458 $ppb^{-1}\,s^{-1}$, respectively. Eqs. (4), (5), and (8) are combined within PALM to simulate dispersion of NO, NO_2, and O_3.

Fig. 1 shows the computational domain. Five two-dimensional street canyons with an aspect ratio of 1 are considered in the simulation, and the building height (H) and street canyon width (W) are both 20 m. The computational domain size is 200 m × 30 m × 99 m in the x-, y-, and z-directions. The grid intervals in the x- and y-directions are 0.25 m, and the grid interval in the z-direction is 0.25 m up to z = 40 m. Above z = 40 m, the grid interval in the z-direction increases by an expansion factor of 1.08 until it becomes 0.5 m. At the upwind (x = 0 m) and downwind (x = 200 m) boundaries, the cyclic boundary condition for velocity is applied. For reactive pollutant concentrations, the Dirichlet and radiation boundary conditions are applied at the upwind and downwind boundaries, respectively. The cyclic boundary condition is imposed for velocity and reactive pollutant concentrations at the side boundaries (y = 0 m and 30 m). Following Park et al. (2012), Monin-Obukhov similarity is employed in the momentum equation and the pollutant transport equations at the grid points closest to the solid surfaces. At the top boundary (z = 99 m), the Dirichlet boundary condition for velocity and the Neumann boundary condition for reactive

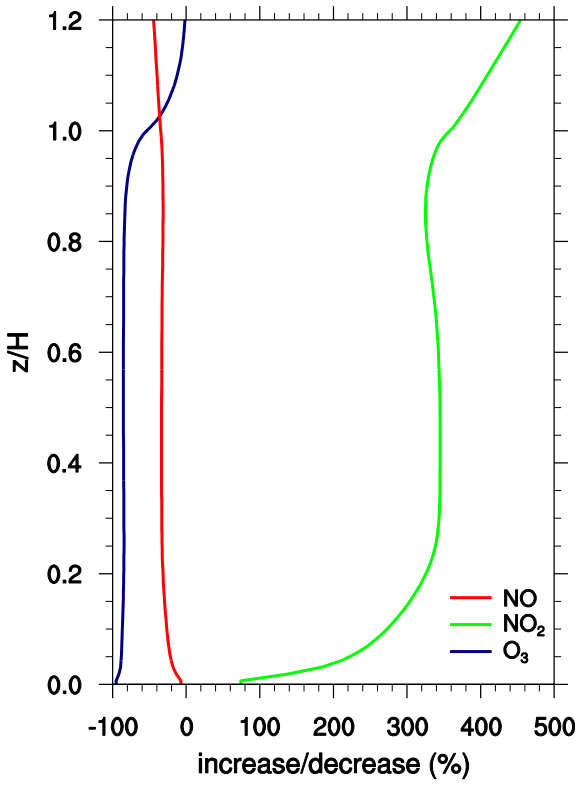

Fig. 4. Vertical profiles of the increase/decrease of mean NO, NO_2, and O_3 concentrations due to the chemical reactions.

pollutant concentrations are imposed. The ambient wind is directed along the x-direction, and a constant wind profile with a speed of $3\,m\,s^{-1}$ is considered as the initial ambient wind profile. Isothermal condition is considered in the simulation, and the temperatures of air, building surface, and canyon floor are 300 K.

For reactive pollutant dispersion, an area source located at the center of the computational domain is considered (Fig. 1), and the emission height is the lowest model level ($z = 0.125$ m). NO and NO_2 are emitted at each grid cell in the area source with uniform pollutant fluxes of 40 ppb $cell^{-1}$ s^{-1} (640 ppb m^{-2} s^{-1}) and 4 ppb $cell^{-1}$ s^{-1} (64 ppb m^{-2} s^{-1}), respectively. Initial background and inflow NO and NO_2 concentrations are 0 ppb. According to Baker et al. (2004), a NO_x emission rate is 0.5 g km^{-1} per vehicle, thus the NO_x emission rate in this study (281 μg s^{-1} m^{-1}) corresponds to 2025 vehicles per hour. Initial background and inflow O_3 concentrations are both 100 ppb. The LES model is run for 2 h, and data of the initial 90 min are excluded from the analysis for spin-up of the LES model. Flow and reactive pollutant concentrations in the street canyon are in a quasi-steady state for the final 30 min. Data of the final 30 min are analyzed in this study.

3. Results and discussion

3.1. Model validation

The present model for reactive pollutant dispersion should be validated using experiment data. However, direct validation of the model is not possible because there is no experiment that measures NO, NO_2, and O_3 concentrations in idealized street canyons. Instead, passive scalar concentration measurement of wind tunnel experiment and the sum of NO and NO_2 concentrations in this simulation are compared for validation. In the transport equations of NO and NO_2 (Eqs. (4) and (5)), the chemical reaction terms are identical but with opposite signs. Therefore, the chemical reaction terms disappear when the two equations are added, and the sum of NO and NO_2 concentrations can be regarded as passive pollutant concentration (Kikumoto and Ooka, 2012).

Fig. 2 shows vertical profiles of sum of time-averaged NO and NO_2 concentrations in the simulation and passive scalar concentration measured in the wind tunnel experiment (Pavageau and Schatzmann, 1999) near the windward and leeward walls (at a distance of $0.03H$ from each wall). Here, the final 30 min data are used for the temporal average of the simulation. It is noted that the 30 min, the averaging time, is much larger than the turnover time of primary circulation (Cai et al., 2008) and the flow-through time. The wind tunnel experiment of Pavageau and Schatzmann (1999) considered a line source located at the center of the street canyon. Therefore, a simulation with a line source in a street canyon is performed for the validation. The results of the simulation and the wind tunnel experiment are normalized by the concentration near the leeward wall at $z = 0.08H$ (Kikumoto and Ooka, 2012). The model slightly overestimates the pollutant concentration except near the ground. It seems that unresolved small-scale turbulence in the model and different turbulent characteristics of inflow between the simulation and the wind tunnel experiment cause the overestimation. In spite of the small overestimation, the simulation result and the wind tunnel data show good agreement, indicating that PALM coupled with the transport equations of NO, NO_2, and O_3 can be reliably used to study turbulent flow and reactive pollutant dispersion.

3.2. Mean flow and concentration

Fig. 3 presents fields of time-averaged mean velocity vector, NO, NO_2, and O_3 concentrations, and the O_3 production rate ($J_{NO_2}\overline{[NO_2]} - k_1\overline{[O_3]}\overline{[NO]}$) on the x–z plane at $y = 15$ m. A large clockwise-rotating vortex appears in the street canyon, and the reactive pollutants are transported by the large vortex. NO and NO_2 are emitted near the ground and transported to the leeward wall (Fig. 3a and b). Then, NO and NO_2 escape from the canyon at the roof level. O_3 enters the street canyon at the roof level, after which O_3 is transported downward along the windward wall (Fig. 3c). These results are consistent with those of Baker et al. (2004) and Baik et al. (2007). In and above the canyon, the mean O_3 production rate is mostly negative (Fig. 3d). This is because NO concentration is higher than that of NO_2. Due to higher NO concentration, the magnitude of the second term of the O_3 production rate ($-k_1\overline{[O_3]}\overline{[NO]}$) is larger than that of the first term ($J_{NO_2}\overline{[NO_2]}$). Additionally, the magnitude of the mean O_3 production rate is large at and near the roof level and near the windward wall. At the roof level, air outside the canyon with high O_3 concentration enters the canyon and mixes with air inside the canyon with high NO concentration. As a result, the magnitude of the second term of the O_3 production rate ($-k_1\overline{[O_3]}\overline{[NO]}$) becomes large and so does the magnitude of the mean O_3 production rate.

To evaluate the effects of the chemical reactions on the mean NO, NO_2, and O_3 concentrations, an additional simulation without the chemical reactions is conducted. For a quantitative comparison between the two simulations, the increase/decrease (in %) of mean reactive pollutant concentration due to the chemical reactions is calculated using:

$$\mathrm{CE} = \frac{<\overline{c}_{\mathrm{chem}}> - <\overline{c}_{\mathrm{nochem}}>}{<\overline{c}_{\mathrm{nochem}}>} \times 100. \tag{9}$$

Here, $\overline{c}_{\mathrm{chem}}$ and $\overline{c}_{\mathrm{nochem}}$ represent reactive pollutant concentrations in the simulations with and without the chemical reactions, respectively. Angle bracket represents the temporal and horizontal average. The horizontal average is taken over $90\,m \le x \le 110$ m and $0\,m \le y \le 30$ m. Fig. 4 shows vertical profiles of CE of NO, NO_2, and O_3. The mean NO and O_3 concentrations in the street canyon decrease by 31% and 84% due to the chemical reactions, respectively. The mean NO_2 concentration in the street canyon increases by 318% because of the chemical reactions. In the street canyon, NO concentration is higher than NO_2 concentration due to large emission rate of NO, i.e., NO has a larger

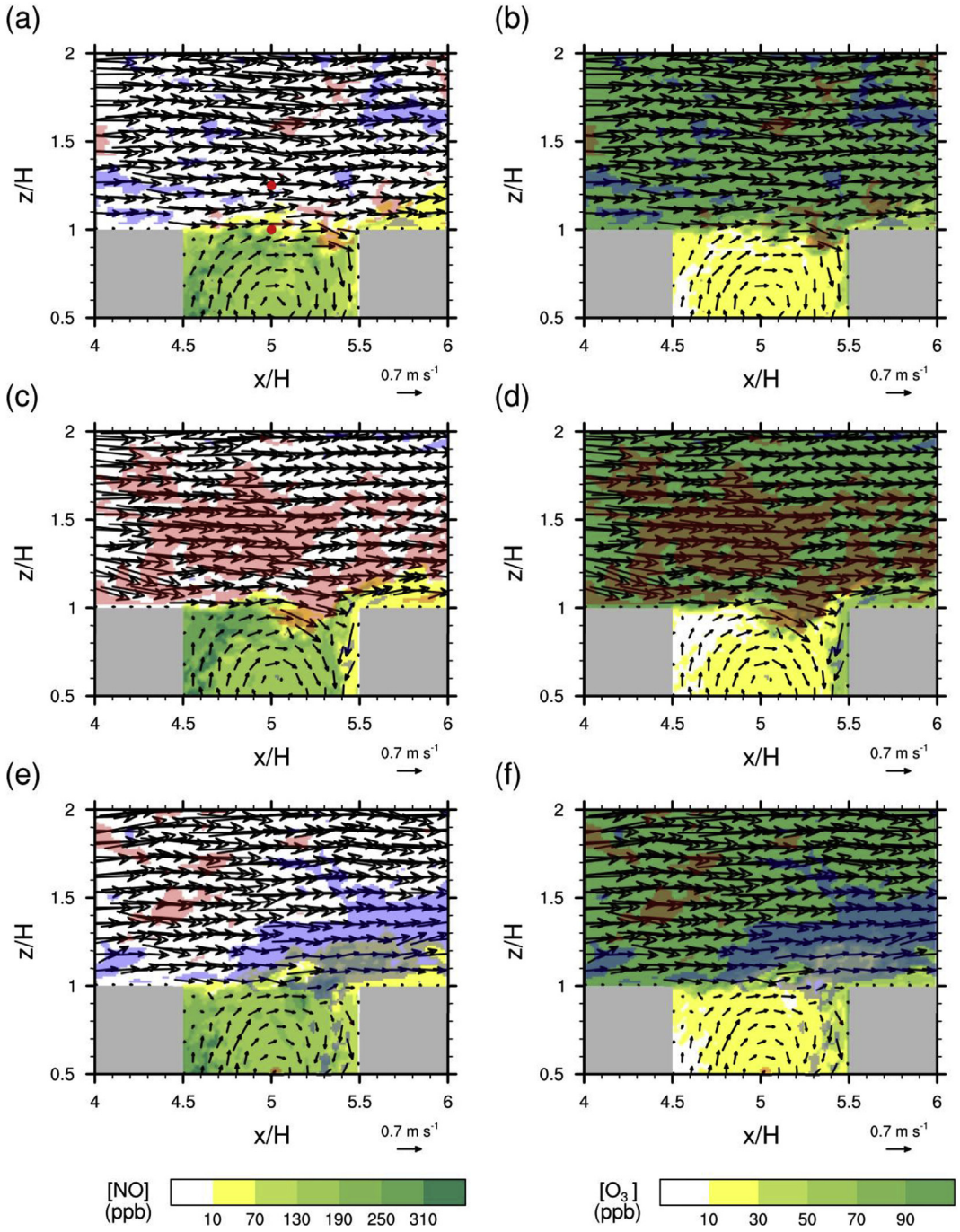

Fig. 5. Fields of velocity vector, NO concentration (left column), and O_3 concentration (right column) at t = (a, b) 5559, (c, d) 5841, and (e, f) 6626 s. Red and blue areas represent the regions where u' is larger than 0.2 m s^{-1} and less than -0.2 m s^{-1}, respectively. Red dots in (a) indicate the locations of u for the two-point time-lagged correlation calculation.

denominator in Eq. (9) than NO_2. As a result, the magnitude of CE of NO is smaller than that of NO_2. Near the ground, the magnitudes of CE of NO and NO_2 decrease because of high NO and NO_2 concentrations near the ground. On the other hand, near the ground, the magnitude of CE of O_3 increases. High NO and NO_2 concentrations near the ground cause the vigorous decomposition of O_3, contributing to the increase of the magnitude of CE of O_3.

3.3. Turbulent flow and concentration

In this subsection, the effects of turbulence on reactive pollutant exchange and the chemical reactions are investigated. Fig. 5 shows fields of velocity vector, NO concentration, and O_3 concentration on the x–z plane at y = 15 m at t = 5559, 5841, and 6626 s. Red and blue areas represent the regions where u' is larger than 0.2 m s^{-1} and less than -0.2 m s^{-1}, respectively. Fields of NO_2 concentration are omitted because the distribution patterns of NO_2 concentration are very similar to those of NO concentration. In this study, the perturbation is defined as a difference between a temporally non-averaged variable and the temporally averaged variable.

In Fig. 5a and b, small eddies appear at the roof level. These small eddies are produced due to the strong wind shear at the roof level. For convenience, these small eddies at the roof level is named small-scale eddies because the size of these eddies are smaller than that of low- or

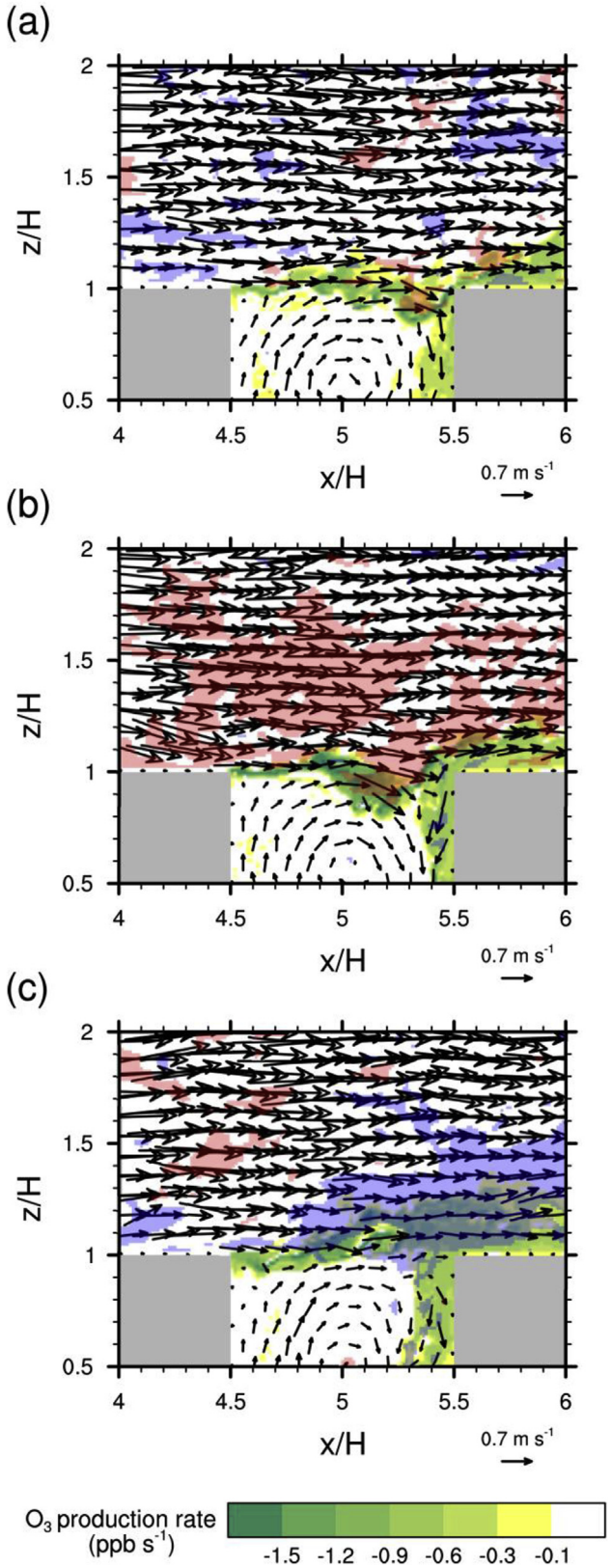

Fig. 6. Fields of velocity vector and the O_3 production rate at t = (a) 5559, (b) 5841, and (c) 6626 s. Red and blue areas represent the regions where u' is larger than 0.2 m s^{-1} and less than −0.2 m s^{-1}, respectively.

high-speed streaks above the canyon in Fig. 5c–f. In Fig. 5a and b, small-scale eddies mainly induce sweep event that transports high-speed air parcel ($u' > 0$) downward ($w' < 0$). As a result, air outside the canyon with high O_3 concentration enters the canyon. Though small-scale eddies in Fig. 5a and b mainly induce sweeps, other small-scale eddies at different times induce ejection event that transports low-speed air parcel ($u' < 0$) upward ($w' > 0$). As a result, air in the canyon with high NO concentration escapes from the canyon. When high-speed streak appears above the canyon, sweep is induced and the entrance of air outside the canyon with high O_3 concentration occurs (Fig. 5c and d). In contrast, low-speed streak above the canyon causes ejection event, and air in the canyon with high NO concentration escapes from the canyon (Fig. 5e and f). Here, low- and high-speed air parcels above the canyon in Fig. 5c–f are named low- and high-speed streaks, respectively, because they show streaky structures on the x–y plane. In general, the majority of low- and high-speed air parcels above the canyon exhibit streaky structures. Low- and high-speed streaks above the canyon are also reported in Kanda (2006). In Fig. 5, larger amounts of reactive pollutants are exchanged at the roof level when low- or high-speed streaks appear above the canyon. It seems that the effect of low- or high-speed streaks above the canyon on reactive pollutant exchange is larger than that of small-scale eddies at the roof level. This result is consistent with that of Michioka et al. (2011).

Fig. 6 shows fields of velocity vector and the O_3 production rate on the x–z plane at y = 15 m at t = 5559, 5841, and 6626 s. The magnitude of the O_3 production rate is large in the region where reactive pollutant exchange occurs. Small-scale eddies at the roof level induce mixing between airs in and above the canyon, and large negative values of the O_3 production rate are seen at the place of this mixing (Fig. 6a). Additionally, vigorous ozone decomposition occurs in the region where air escapes from or enters the canyon when low- or high-speed streaks appear above the canyon, respectively (Fig. 6b and c). Therefore, we conclude that small-scale eddies at the roof level and low- or high-speed streaks above the street canyon increase the magnitude of the O_3 production rate. The magnitude of the O_3 production rate is large at the edge of the region where air escapes from or enters the canyon because NO and O_3 are mixed more thoroughly at the edge of the region than at the center of the region. This incomplete mixing is also reported in Garmory et al. (2009) and Zhong et al. (2017).

The effects of small-scale eddies at the roof level and low- or high-speed streaks above the canyon on reactive pollutant exchange at the roof level are investigated further using the joint probability density function (JPDF), which is defined as follows:

$$f_{a,b}(x_i, y_j) = P(x_i - 0.5\Delta x < a \leq x_i + 0.5\Delta x, \; y_j - 0.5\Delta y < b \leq y_j + 0.5\Delta y). \quad (10)$$

Here, a and b are the variables, x_i and Δx are the center and spacing of bins for the variable a, and y_j and Δy are the center and spacing of bins for the variable b (Park and Baik, 2013).

Fig. 7 shows fields of the JPDF of u' and w', NO and O_3 concentration perturbations, and the O_3 production rate on the x–y plane at the roof level. Here, u and w represent the velocities in the x- and z-directions, respectively. Prime denotes the perturbation. The spacings of bins for u' and w' are both 0.04 m s^{-1}. The spacings of bins for NO and O_3 concentration perturbations and the O_3 production rate are 14 ppb, 4 ppb, and 0.18 ppb s^{-1}, respectively. At the roof level, ejection events that transport low-speed air parcel ($u' < 0$) upward ($w' > 0$) and sweep events that transport high-speed air parcel ($u' > 0$) downward ($w' < 0$) are the most dominant events (Fig. 7a). Ejections occur the most frequently, while sweeps occur with the strongest magnitude of events. These results are consistent with those of Kikumoto and Ooka (2012). Small-scale eddies at the roof level and low- or high-speed streaks above the canyon induce strong ejections or sweeps (Fig. 5 and 6) and significantly affect flow at the roof level.

NO and O_3 concentration perturbations are significantly affected by ejections and sweeps (Fig. 7b and c). When u' is negative at the roof level, NO and O_3 concentration perturbations are generally positive and negative, respectively, due to the upward motion of ejections.

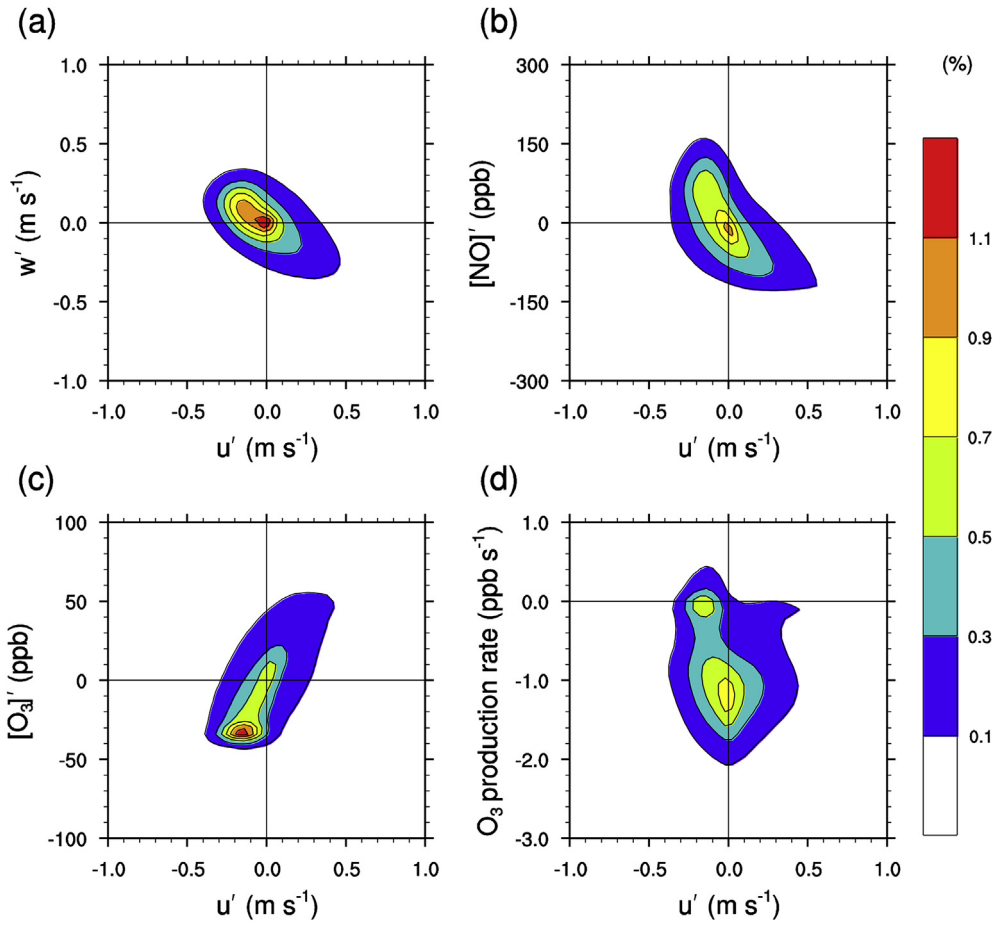

Fig. 7. Fields of the joint probability density function of u' and (a) w', (b) NO and (c) O_3 concentration perturbations, and (d) the O_3 production rate. The data at z = 20 m are used.

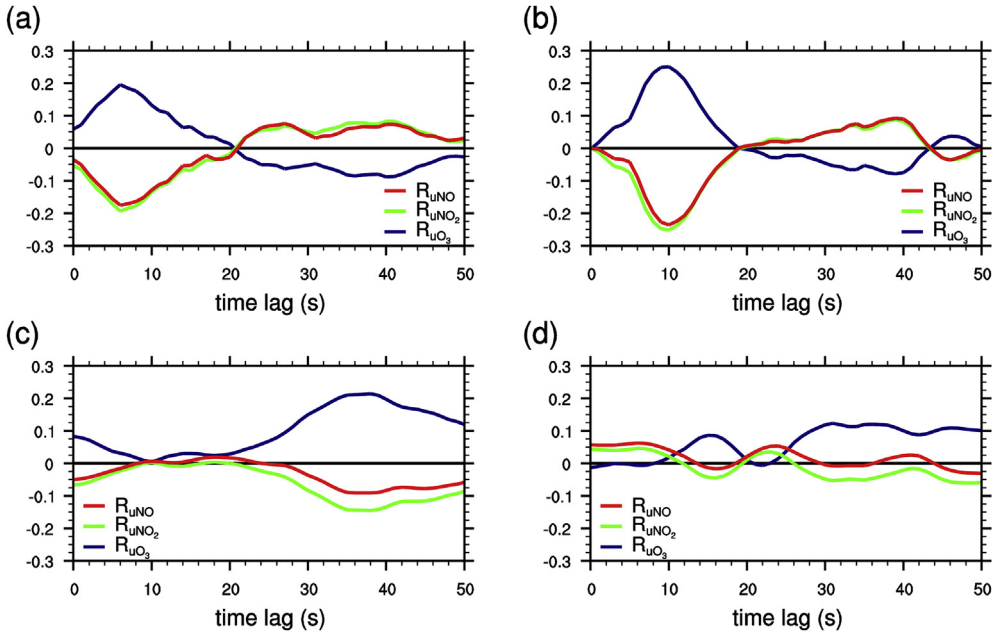

Fig. 8. Graphs of time-lagged correlations between u at points (x, y, z) = (100 m, 15 m, 25 m) (left column) and (100 m, 15 m, 20 m) (right column) and NO, NO_2, and O_3 concentrations at points (a, b) (x, y, z) = (108 m, 15 m, 20 m) and (c, d) (x, y, z) = (108 m, 15 m, 2 m).

Conversely, when u' is positive at the roof level, sweeps usually occur and the downward motion of sweeps causes negative NO and positive O_3 concentration perturbations. According to characteristics of ejection, the occurrence frequencies of NO and O_3 concentration perturbations are large when u' is negative at the roof level. In Fig. 7d, the JPDF of u' and the O_3 production rate is concentrated at (u', O_3 production rate) ~ ($-0.15\ m\ s^{-1}$, $-0.1\ ppb\ s^{-1}$) and ($0\ m\ s^{-1}$, $-1.2\ ppb\ s^{-1}$). When frequent ejections occur, the low O_3 production rate ($-0.1\ ppb\ s^{-1}$) appears at the center of the region where air escapes from the canyon. Ejections occur frequently at the roof level, so that the occurrence frequency becomes high at (u', O_3 production rate) ~ ($-0.15\ m\ s^{-1}$, $-0.1\ ppb\ s^{-1}$). The occurrence frequency at (u', O_3 production rate) ~ ($0\ m\ s^{-1}$, $-1.2\ ppb\ s^{-1}$) is high because vigorous O_3 decomposition occurs at the edge of the region where air escapes from or enters the canyon, with small magnitudes of u' at the edge of the region.

To differentiate between the effect of small-scale eddies at the roof level and the effect of low- or high-speed streaks above the canyon, the two-point time-lagged correlation is calculated using the following:

$$R_{\alpha\beta} = \frac{<\alpha'(x_1,\ y_1,\ z_1,\ t)\beta'(x_2,\ y_2,\ z_2,\ t+\tau)>}{\sqrt{<(\alpha'(x_1,\ y_1,\ z_1,\ t))^2>}\sqrt{<(\beta'(x_2,\ y_2,\ z_2,\ t))^2>}}. \quad (11)$$

Here, τ represents the time lag, and (x_1, y_1, z_1) and (x_2, y_2, z_2) represent the locations of the variables α and β, respectively. Eq. (11) is used to calculate a correlation between the variable α at (x_1, y_1, z_1) and the variable β at (x_2, y_2, z_2) with the time lag τ.

Fig. 8 shows graphs of time-lagged correlations between u at points (x, y, z) = (100 m, 15 m, 25 m) and (100 m, 15 m, 20 m) and NO, NO_2, and O_3 concentrations at points (x, y, z) = (108 m, 15 m, 20 m) and (108 m, 15 m, 2 m). The locations of u are at $z = H$ and $1.25H$ along the vertical line of the canyon center (red dots in Fig. 5a). At $z = 1.25H$, u is located sufficiently high, so that small-scale eddies at the roof level non-significantly affect u at that level. Therefore, the time-lagged correlations with u at $z = 1.25H$ are regarded as representing the effect of low- or high-speed streaks above the canyon. The locations of NO, NO_2, and O_3 concentrations are at a distance of $0.1H$ from the windward wall at $z = H$ and $0.1H$. For convenience, the time-lagged correlation between α at $z = z_1$ and β at $z = z_2$ is denoted as $R_{\alpha\beta}(z_1,\ z_2)$.

$R_{uNO}(1.25H,\ H)$ and $R_{uNO_2}(1.25H,\ H)$ in Fig. 8a and $R_{uNO}(H,\ H)$ and $R_{uNO_2}(H,\ H)$ in Fig. 8b have negative peaks, while $R_{uO_3}(1.25H,\ H)$ in Fig. 8a and $R_{uO_3}(H,\ H)$ in Fig. 8b have positive peaks. This means that air with negative u' due to small-scale eddies at the roof level or low-speed streak above the canyon induces the escape of pollutants from the canyon, resulting in positive NO and NO_2 and negative O_3 concentration perturbations at the roof level. Similarly, when air with positive u' appears due to small-scale eddies at the roof level or high-speed streak above the canyon, air frequently enters the canyon and negative NO and NO_2 and positive O_3 concentration perturbations are seen at the roof level. The magnitudes of the peaks of $R_{uNO}(H,\ H)$, $R_{uNO_2}(H,\ H)$, and $R_{uO_3}(H,\ H)$ are larger than those of $R_{uNO}(1.25H,\ H)$, $R_{uNO_2}(1.25H,\ H)$, and $R_{uO_3}(1.25H,\ H)$, respectively. This is because small-scale eddies at the roof level as well as low- or high-speed streaks above the canyon induce reactive pollutant exchange at $z = H$. In Fig. 8c, $R_{uNO}(1.25H,\ 0.1H)$, $R_{uNO_2}(1.25H,\ 0.1H)$, and $R_{uO_3}(1.25H,\ 0.1H)$ show peaks. This means that low- or high-speed streaks above the canyon affect NO, NO_2, and O_3 concentrations not only at the roof level but also near the ground ($z = 0.1H$). $R_{uNO}(1.25H,\ H)$, $R_{uNO_2}(1.25H,\ H)$, and $R_{uO_3}(1.25H,\ H)$ have peaks at a time lag of ~6 s, while $R_{uNO}(1.25H,\ 0.1H)$, $R_{uNO_2}(1.25H,\ 0.1H)$, and $R_{uO_3}(1.25H,\ 0.1H)$ have peaks at a time lag of ~37 s. $R_{uNO}(H,\ 0.1H)$, $R_{uNO_2}(H,\ 0.1H)$, and $R_{uO_3}(H,\ 0.1H)$ do not show clear peaks (Fig. 8d). It seems that small-scale eddies at the roof level non-significantly affect NO, NO_2 and O_3 concentrations near the ground.

4. Summary and conclusions

We investigated the exchange of reactive pollutants at the roof level of an urban street canyon using an LES model. NO, NO_2, and O_3 are concerned in the LES model, and their transport equations with simple photochemical reactions are combined within the model. A large clockwise-rotating vortex in the street canyon transports the reactive pollutants. As a result, NO and NO_2 emitted near the ground are transported along the leeward wall and escape from the canyon at the roof level. O_3 in the ambient air enters the canyon at the roof level and is transported along the windward wall. The mean O_3 production rate is mostly negative both in and above the canyon, and the magnitude of the O_3 production rate is large at and near the roof level and near the windward wall. Due to the photochemical reactions of NO, NO_2, and O_3, the mean NO and O_3 concentrations in the canyon decrease by 31% and 84%, respectively. The chemical reactions result in an increase of 318% in the mean NO_2 concentration in the canyon.

Both small-scale eddies at the roof level and low- or high-speed streaks above the canyon significantly affect the exchange of reactive pollutants at the roof level. When low-speed air parcel appears at the roof level due to small-scale eddies or low-speed streak above the canyon, air in the canyon with high NO and NO_2 concentrations frequently escapes from the canyon. On the other hand, air outside the canyon with high O_3 concentration frequently enters the canyon when high-speed air parcel appears at the roof level due to small-scale eddies at the roof level or high-speed streak above the canyon. When air escapes from or enters the canyon, the magnitude of the O_3 production rate becomes large. The analysis of the JPDF also confirms the effects of small-scale eddies at the roof level and low- or high-speed streaks above the canyon on the exchange of reactive pollutants and their chemical reactions. It seems that low- or high-speed streaks above the canyon have a greater influence than small-scale eddies at the roof level, i.e., air is exchanged more substantially when low- or high-speed streaks appear above the canyon. Additionally, the two-point time-lagged correlation analysis shows that both small-scale eddies at the roof level and low- or high-speed streaks above the canyon affect NO, NO_2, and O_3 concentrations at the roof level. However, only low- or high-speed streaks above the canyon significantly affect NO, NO_2, and O_3 concentrations near the ground.

This study investigated the exchange of reactive pollutants and their associated photochemical reactions at the roof level of a street canyon. This study considers only the simple photochemical reactions of NO, NO_2, and O_3. Concentrations and chemical reactions of reactive pollutants are changed when complex chemical processes are considered (Zhong et al., 2017). Therefore, further studies that consider real complex chemical processes need to be conducted to better understand reactive pollutant exchange processes in urban areas. In addition, the effects of heating in a street canyon and ambient wind direction on reactive pollutant exchange need to be investigated. Variations in the emission rates of NO and NO_2 and the ambient O_3 concentration can affect reactive pollutant exchange, deserving future in-depth investigations.

Acknowledgements

The authors are grateful to two anonymous reviewers for providing valuable comments on this work. This work was supported by Basic Science Research Program through the National Research Foundation of Korea (NRF) funded by the Ministry of Science and ICT (No. 2016R1A2B2013549).

References

Allegrini, J., Dorer, V., Carmeliet, J., 2013. Wind tunnel measurements of buoyant flows in street canyons. Build. Environ. 59, 315–326.

Allwine, K.J., Shinn, J.H., Streit, G.E., Clawson, K.L., Brown, M., 2002. Overview of URBAN 2000: a multiscale field study of dispersion through an urban environment. Bull. Am. Meteorol. Soc. 83, 521–536.

Baik, J.-J., Kim, J.-J., 2002. On the escape of pollutants from urban street canyons. Atmos. Environ. 36, 527–536.

Baik, J.-J., Kang, Y.-S., Kim, J.-J., 2007. Modeling reactive pollutant dispersion in an urban street canyon. Atmos. Environ. 41, 934–949.
Baker, J., Walker, H.L., Cai, X., 2004. A study of the dispersion and transport of reactive pollutants in and above street canyons—a large eddy simulation. Atmos. Environ. 38, 6883–6892.
Cai, X.-M., Barlow, J.F., Belcher, S.E., 2008. Dispersion and transfer of passive scalars in and above street canyons—large-eddy simulations. Atmos. Environ. 42, 5885–5895.
Chung, T.N.H., Liu, C.-H., 2013. On the mechanism of air pollutant removal in two-dimensional idealized street canyons: a large-eddy simulation approach. Boundary-Layer Meteorol. 148, 241–253.
Cui, Z., Cai, X., Baker, C.J., 2004. Large-eddy simulation of turbulent flow in a street canyon. Q. J. R. Meteorol. Soc. 130, 1373–1394.
Deardorff, J.W., 1980. Stratocumulus-capped mixed layers derived from a three-dimensional model. Boundary-Layer Meteorol. 18, 495–527.
Garmory, A., Kim, I.S., Britter, R.E., Mastorakos, E., 2009. Simulations of the dispersion of reactive pollutants in a street canyon, considering different chemical mechanisms and micromixing. Atmos. Environ. 43, 4670–4680.
Grawe, K., Cai, X.-M., Harrison, R.M., 2007. Large eddy simulation of shading effects on NO_2 and O_3 concentrations within an idealised street canyon. Atmos. Environ. 41, 7304–7314.
Kanda, M., 2006. Large-eddy simulations on the effects of surface geometry of building arrays on turbulent organized structures. Boundary-Layer Meteorol. 118, 151–168.
Kastner-Klein, P., Fedorovich, E., Rotach, M.W., 2001. A wind tunnel study of organised and turbulent air motions in urban street canyons. J. Wind Eng. Ind. Aerodyn. 89, 849–861.
Kikumoto, H., Ooka, R., 2012. A numerical study of air pollutant dispersion with bimolecular chemical reactions in an urban street canyon using large-eddy simulation. Atmos. Environ. 54, 456–464.
Kim, M.J., Park, R.J., Kim, J.-J., 2012. Urban air quality modeling with full O_3-NO_x-VOC chemistry: implications for O_3 and PM air quality in a street canyon. Atmos. Environ. 47, 330–340.
Kwak, K.-H., Baik, J.-J., 2012. A CFD modeling study of the impacts of NO_x and VOC emissions on reactive pollutant dispersion in and above a street canyon. Atmos. Environ. 46, 71–80.
Kwak, K.-H., Baik, J.-J., 2014. Diurnal variation of NO_x and ozone exchange between a street canyon and the overlying air. Atmos. Environ. 86, 120–128.
Letzel, M.O., Krane, M., Raasch, S., 2008. High resolution urban large-eddy simulation studies from street canyon to neighbourhood scale. Atmos. Environ. 42, 8770–8784.
Li, X.-X., Liu, C.-H., Leung, D.Y.C., Lam, K.M., 2006. Recent progress in CFD modelling of wind field and pollutant transport in street canyons. Atmos. Environ. 40, 5640–5658.
Liu, C.-H., Wong, C.C.C., 2014. On the pollutant removal, dispersion, and entrainment over two-dimensional idealized street canyons. Atmos. Res. 135–136, 128–142.
Maronga, B., Gryschka, M., Heinze, R., Hoffmann, F., Kanani-Sühring, F., Keck, M., Ketelsen, K., Letzel, M.O., Sühring, M., Raasch, S., 2015. The Parallelized Large-Eddy Simulation Model (PALM) version 4.0 for atmospheric and oceanic flows: model formulation, recent developments, and future perspectives. Geosci. Model Dev. 8, 2515–2551.
Michioka, T., Sato, M., Takimoto, H., Kanda, M., 2011. Large-eddy simulation for the mechanism of pollutant removal from a two-dimensional street canyon. Boundary-Layer Meteorol. 138, 195–213.
Moradpour, M., Afshin, H., Farhanieh, B., 2018. A numerical study of reactive pollutant dispersion in street canyons with green roofs. Build. Simul. 11, 125–138.
Nelson, M.A., Pardyjak, E.R., Klein, P., 2011. Momentum and turbulent kinetic energy budgets within the Park Avenue street canyon during the Joint Urban 2003 field campaign. Boundary-Layer Meteorol. 140, 143–162.
Park, S.-B., Baik, J.-J., Raasch, S., Letzel, M.O., 2012. A large-eddy simulation study of thermal effects on turbulent flow and dispersion in and above a street canyon. J. Appl. Meteorol. Climatol. 51, 829–841.
Park, S.-B., Baik, J.-J., 2013. A large-eddy simulation study of thermal effects on turbulence coherent structures in and above a building array. J. Appl. Meteorol. Climatol. 52, 1348–1365.
Park, S.-J., Kim, J.-J., Kim, M.J., Park, R.J., Cheong, H.-B., 2015. Characteristics of flow and reactive pollutant dispersion in urban street canyons. Atmos. Environ. 108, 20–31.
Pavageau, M., Schatzmann, M., 1999. Wind tunnel measurements of concentration fluctuations in an urban street canyon. Atmos. Environ. 33, 3961–3971.
Rotach, M.W., 1995. Profiles of turbulence statistics in and above an urban street canyon. Atmos. Environ. 29, 1473–1486.
Sanchez, B., Santiago, J.-L., Martilli, A., Palacios, M., Kirchner, F., 2016. CFD modeling of reactive pollutant dispersion in simplified urban configurations with different chemical mechanisms. Atmos. Chem. Phys. 16, 12143–12157.
Seinfeld, J.H., Pandis, S.N., 2006. Atmospheric Chemistry and Physics: from Air Pollution to Climate Change. John Wiley & Sons, Inc., USA.
Shetter, R.E., Davidson, J.A., Cantrell, C.A., Burzynski Jr., N.J., Calvert, J.G., 1988. Temperature dependence of the atmospheric photolysis rate coefficient for NO_2. J. Geophys. Res. 93, 7113–7118.
Wicker, L.J., Skamarock, W.C., 2002. Time-splitting methods for elastic models using forward time schemes. Mon. Weather Rev. 130, 2088–2097.
Zhong, J., Cai, X.-M., Bloss, W.J., 2015. Modelling the dispersion and transport of reactive pollutants in a deep urban street canyon: using large-eddy simulation. Environ. Pollut. 200, 42–52.
Zhong, J., Cai, X.-M., Bloss, W.J., 2016. Coupling dynamics and chemistry in the air pollution modelling of street canyons: a review. Environ. Pollut. 214, 690–704.
Zhong, J., Cai, X.-M., Bloss, W.J., 2017. Large eddy simulation of reactive pollutants in a deep urban street canyon: coupling dynamics with O_3-NO_x-VOC chemistry. Environ. Pollut. 224, 171–184.